

Artifacts in measurements of chlorophyll fluorescence transients, with specific application to fast repetition rate fluorometry

Samuel R. Laney* and Ricardo M. Letelier

College of Oceanic & Atmospheric Sciences, Oregon State University, Corvallis, OR 97331-5503 USA

Abstract

A theoretical framework was developed to describe how instrument and sample artifacts affect measurements of variable fluorescence transients in phytoplankton. This framework identified the proper procedure for correcting for common artifacts in the transients measured with a widely used instrument, the Fasttrack fast repetition rate fluorometer. The impulse response of this fluorometer can be substantial, requiring correction for a dynamic instrument artifact in addition to the static artifacts that can be assessed using traditional “blanks.” In a low-biomass region of the North Pacific, approximately one-third of the fluorescence transient measured with this instrument represented such artifacts. Correcting for these using filtered seawater blanks only, and not accounting for the instrument’s own response, failed to remove errors as high as 22% in estimates in the photochemical yield and as much as –16% to +22% in estimates of the functional cross section of Photosystem II. This analytical framework and the corrective procedure are generalized and can be used to determine how a wide range of artifacts affect measured variable fluorescence transients, including those characteristic of fluorometers other than the Fasttrack or those more relevant in meso- or eutrophic regions of the ocean.

The yield of chlorophyll fluorescence F in plants and algae is controlled in part by the redox state of the primary electron acceptor Q_A . When all Q_A are oxidized, the fraction of absorbed photons dissipated via photochemistry is maximal and, as a result, F is minimal. Conversely, when Q_A is fully reduced, F will be maximal because additionally absorbed photons cannot be dissipated photochemically. These yields can be measured in dark adapted samples by adding an herbicide such as DCMU, which alters F from its minimum (F_o) to its maximum (F_m). These yields are important parameters in photosynthesis research because a derived property, $(F_m - F_o) \times F_m^{-1}$, is a proxy for the quantum yield of photochemistry (Genty et al. 1989). The numerator of this ratio is the variable fluorescence yield, often denoted as F_v .

These same yields also can be measured noninvasively, without herbicides, by forcing F from F_o to F_m photochemi-

cally using brief, intense flashes of light. Several methods have been developed for measuring F_o and F_m in this way, some specifically for oceanographic use. These include “pump-and-probe” fluorometry (Mauzerall 1972; Falkowski et al. 1986), “fast repetition rate” (FRR) fluorometry (Kolber et al. 1998), “pump-during-probe” (PDP) fluorometry (Olson et al. 1996), and other techniques that are similar functionally (e.g., Koblížek et al. 2001; Fuchs et al. 2002; Johnson 2004). With the pump-and-probe method, a single intense “pump” flash oxidizes all Q_A nearly instantaneously and “probe” measurements of F before and after this flash determine F_o and F_m respectively. In the other methods, Q_A is photochemically oxidized gradually over a period of tens to hundreds of μ s, shorter than the many-ms “single-turnover” time scale of Photosystem II (PSII). The kinetics of the resulting transient increase from F_o to F_m contain photosynthetic information beyond just these two yields. The functional cross-section of PSII (σ_{PSII}) can be estimated from these kinetics, and their deviation from a simple Stern-Volmer model of fluorescence quenching presumably reflects some degree of energetic connectivity between PSII (Ley and Mauzerall 1986; Kolber et al. 1998).

Typically, these fluorescence transients $F(t)$ are not determined directly but instead are computed from separate measurements of the transient fluorescence emission $EM(t)$ and the excitation transient $EX(t)$ that stimulated it. In this scenario,

*Corresponding author, current address: Biology Department, Woods Hole Oceanographic Institution, Redfield 3-16 MS #32, Woods Hole, MA 02543 USA. Phone: 508-289-3647; FAX: 508 457 2134; E-mail: sam@whoi.edu

Acknowledgments

Funding for this research was provided by the National Science Foundation (grant OCE-0326419) and by the National Aeronautics and Space Administration (contract NNG04HZ35C). The authors would like to thank Dave Karl and the Hawaii Ocean Time-series program for supporting our fieldwork at Station ALOHA. Russell Desiderio and two anonymous reviewers provided valuable feedback on drafts of this manuscript.

Table 1. Definitions of terms used in this treatment of artifacts

Artifact	Any aspect of the sample, instrument, or experimental configuration that distorts a measurement.
Sample artifacts	Artifacts that arise due to a property of the sample.
Instrument artifacts	Artifacts that arise due to a property of the instrument.
Static artifacts	Artifacts whose effect is constant over the measurement time scale (here, the duration of a measured EM or EX transient).
Dynamic artifacts	Artifacts whose effect varies during a transient measurement.
Blank	A general term that typically refers to a measurement of static instrument and/or sample artifacts.

$F(t)$ is defined as the ratio of $EM(t)$ to $EX(t)$, i.e., $F(t) = EM(t) \times EX(t)^{-1}$, to account for any apparent changes in $EM(t)$ that result from changes in EX during the transient measurement (Kolber et al. 1998). Photosynthetic parameters such as F_o , F_m' , and σ_{PSII} will be estimated most accurately from this $F(t)$ when its magnitude and kinetics reflect photosynthetic processes alone. In practice, however, this is rarely the case: measured EM and EX transients often are affected by properties of the sample or the instrument used. These introduce artifacts into the $F(t)$ that is computed. For example, if dissolved organic matter in the sample fluoresces in the chlorophyll emission wavelengths, an apparent increase in EM will be observed (e.g., Fuchs et al. 2002). Similarly, ambient or excitation irradiance that is scattered into the fluorescence detector by water, particles, or by the instrument itself also will produce an artifactual increase in EM if this scatterance leaks past excitation blocking filters on the fluorescence detector.

These two particular artifacts vary negligibly on the μs -to- ms time scale of the transient and are effectively “static” (see Table 1) in measurements of $EM(t)$. Static instrument and sample artifacts often can be corrected for algebraically by measuring and subtracting appropriate “blanks” that indicate their magnitude (Cullen and Davis 2003). Other factors might not remain effectively constant during these transient measurements, and such “dynamic” artifacts also must be considered when analyzing variable fluorescence transients. A dynamic artifact can be seen in the $EM(t)$ measured with a widely used fast repetition rate fluorometer, the Fasttracka FRR fluorometer (FRRF, Chelsea Marine Systems), appearing as an increase in $EM(t)$ in the absence of any photosynthetic sample (Fig. 1). This artifact arises from the signal conditioning circuitry that follows the photomultiplier detector and can be predicted from circuit simulations. This artifact does not appear in the concurrent $EX(t)$, which is measured using a photodiode that has different signal conditioning circuitry.

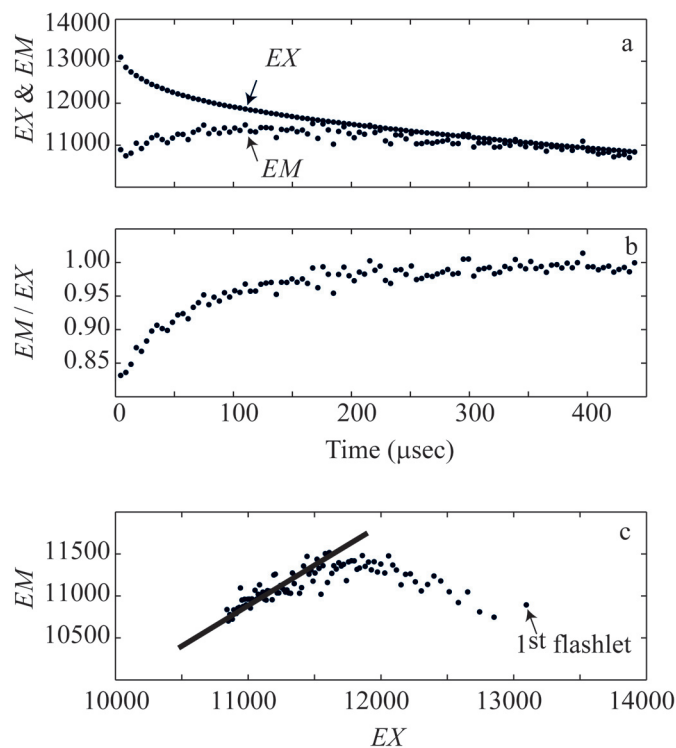


Fig. 1. (a) Example $EX(t)$ and $EM(t)$ from a Fasttracka FRR fluorometer, for a “sample” consisting of a prism and a 1.2 OD neutral density filter placed in the instrument’s “light” chamber. The gradual decrease in EX (instrument units) reflects the discharge of excitation energy from a storage capacitor. (b) The corresponding change in $EM \times EX^{-1}$ over time shows a changing relationship between EM and EX during the first half of the flashlet sequence. Mistakenly interpreting this artifact as reflecting photosynthetic influence would lead to an estimated σ_{PSII} of $\approx 455 \text{ \AA}^2 \text{ photon}^{-1}$. (c) The correlation between these measured EX and EM , with a trend line (Model II linear regression, $r^2 = 0.94$) fit to the final 40 points of the flashlet sequence. Anomalous behavior in the first flashlet can be observed.

Recent identification of widespread instrument artifacts in measurements of ocean temperature (Schiermeier 2007; Willis et al. 2007) serves as a caution for developers and users of oceanographic single-turnover fluorometers, which are more sophisticated comparatively and whose potential artifacts are less well understood. The theory and procedures for correcting for static artifacts in variable fluorescence have been well described (see Cullen and Davis 2003), but a general framework that encompasses both static and dynamic artifacts remains lacking. A previous study indicated that large and poorly constrained errors in F_o , F_m' , and σ_{PSII} will arise when EM transients measured with the Fasttracka fluorometer are not corrected for dynamic artifacts (Laney 2003). The corrective method used in that study improved estimates of F_o , F_m' , and σ_{PSII} in many measurement situations, yet it remains less than ideal for two main reasons. First, it is based on an historically used, yet mathematically inappropriate, description of how dynamic artifacts affect $F(t)$. Second, it provides no insight into the physical bases of these dynamic artifacts. Without a rigorous framework

that quantifies how different types of static and dynamic artifacts affect $F(t)$, it is difficult to determine when an empirical corrective approach is or is not effective.

Proper analysis of both historical and extant $F(t)$ data requires a corrective approach that stands on solid theoretical footing. We developed a general mathematical framework that describes how static and dynamic artifacts affect measurements of $EM(t)$ and thus the $F(t)$ computed from it and from $EX(t)$. Using this framework, we derived a simple and repeatable technique for determining the dynamic artifact of any instrument that measures variable fluorescence transients. We identified a mechanistic model for the specific dynamic artifact seen in the Fasttracka fluorometer and used this model to develop a corrective approach to improve estimates of the photosynthetic parameters derived from its measurements of $EM(t)$ and $EX(t)$. We evaluated this corrective approach in near-surface phytoplankton assemblages in the subtropical North Pacific, where measured F is weak due to low algal biomass and strong non-photochemical quenching. Such conditions are characteristic of much of the surface ocean and require particularly robust corrective approaches to estimate photosynthetic parameters most accurately.

Materials and procedures

Determining how different sources of artifact affect fluorescence transients—A diagrammatic technique commonly used in signal processing and systems analysis can be used to show how various sample and instrument artifacts affect $EM(t)$ and, therefore, $F(t)$. Properly constructed diagrams will indicate the appropriate procedure for correcting $EM(t)$ measurements for any specific combination of artifacts. These diagrams often are presented in the discrete-time domain where signals are described as a function of n , an integer representing the index of a particular datum (e.g., $X[n]$). Fluorescence transients also often are described as discrete-time sequences, either explicitly, as with the ‘flashlets’ in FRR fluorometry, or implicitly when digitizing fluorescence transients. Thus, this diagrammatic technique can be adapted readily to use with the fluorescence transients of phytoplankton by replacing the continuous-time signals $EX(t)$ and $EM(t)$ with their discrete-time equivalents $EX[n]$ and $EM[n]$.

The transfer of a time-varying excitation $EX[n]$ into a fluorescence emission $EM[n]$ is represented by arrows in these diagrams (Fig. 2). Triangles are used to represent factors that only amplify or attenuate this transfer, and their effect can be described by a scalar transfer function A that is equivalent to this gain or loss. Rectangles are used to represent factors whose effect on a signal may vary in time and which cannot be represented using a simple scalar transfer function. By convention, transfer functions are defined as the impulse response $h_i[n]$, a vector.

An example (Fig. 2a) shows how an inert fluorophore, such as a dye, transforms excitation $EX[n]$ into a fluorescence $EM[n]$. Here the fluorophore is represented by a triangle with a scalar transfer function A analogous to its quantum yield. The relationship between EM and EX is expressed by the

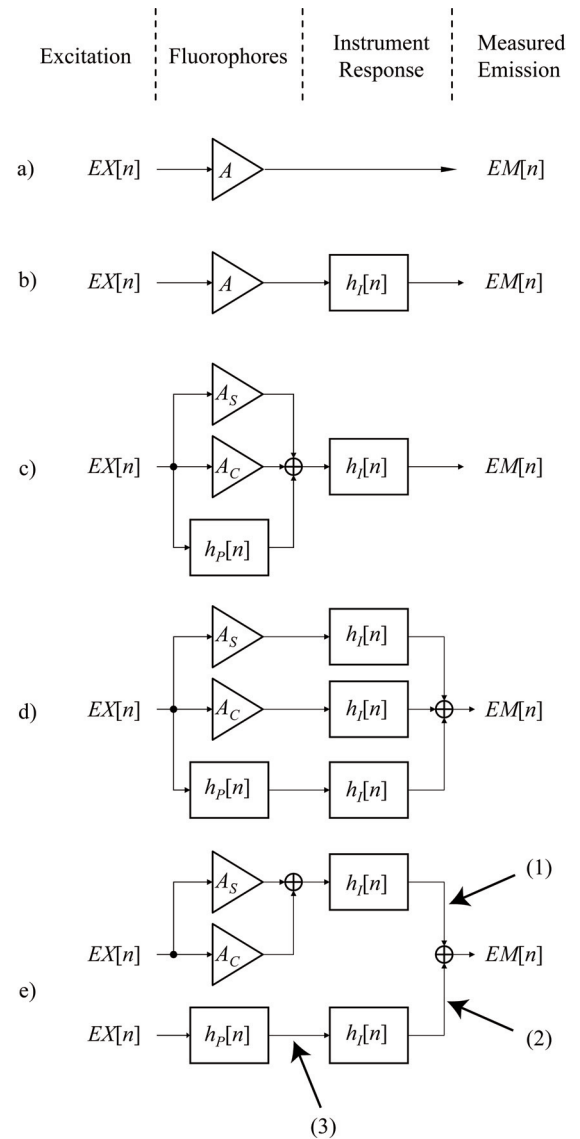


Fig. 2. (a) A simple system of an ideal fluorophore with no inherent fluorescence transient behavior, such as a dye. (b) The same system, measured by an instrument with non-negligible impulse response $h_i[n]$. (c) A more realistic system that includes a phytoplankton term $h_p[n]$ and contributions A_s from instrument self-scatter and A_c from dissolved organic matter fluorescence. (d),(e) Topologically equivalent representations of (c), where arrows refer to signals referenced in the text.

convolution $EM[n] = A * EX[n]$, where we use the symbol ‘*’ to distinguish convolution from multiplication, which we represent with the ‘ \times ’ symbol. Because this transfer function is a scalar, the convolution in this particular example reduces to simple multiplication: $EM(t) = A \times EX(t)$. Thus, the A of this fluorophore can be computed by dividing EM at any datum n or time t by its corresponding $EX[n]$ or $EX(t)$.

A more realistic example is shown in Fig. 2b, where the same fluorophore is again excited by a time-varying excitation

$EX[n]$ but where the emission $EM[n]$ is now measured by an instrument with a non-negligible dynamic response $h_f[n]$. The apparent measured $EM[n]$ signal is the convolution of the true emission $A \times EX[n]$ with the instrument's transfer function $h_f[n]$, i.e., $EM[n] = A \times EX[n] * h_f[n]$. In this situation, time-dependent changes in $EM[n]$ will occur solely as a result of the instrument's response $h_f[n]$. To estimate A properly, both $EX[n]$ and $h_f[n]$ must be deconvolved from the apparent $EM[n]$. Distinguishing when signals are multiplied or convolved is an essential aspect of using signal processing tools and techniques correctly. Static artifacts (resulting from factors with scalar transfer functions) can be corrected for algebraically because these only multiply a signal by some gain or loss. A dynamic artifact, with a vector transfer function, acts on a signal by convolution and thus can be corrected for only through deconvolution. Relevant principles and theory can be found in Doebelin (1990) and in Mitra (2001).

Because phytoplankton affect both the magnitude and kinetics of how EX is transferred into EM , they should be represented in these diagrams by rectangles with vector transfer functions $h_p[n]$. A more oceanographically realistic example (Fig. 2c) shows a sample that contains phytoplankton and two sources of artifact: dissolved fluorescent material in the sample and scatterance of excitation irradiance into the emission detector. These sample artifacts are static and affect only the magnitude with which EX is transferred into EM , so they are represented by triangles and assigned scalar transfer functions A_c and A_s . The transient response in $EM[n]$ of this more realistic sample is the sum of $h_p[n]$, A_c , and A_s , each convolved with $EX[n]$. The signal measured by the instrument is that sum, convolved finally with the instrument artifact $h_f[n]$.

In phytoplankton suspensions that are optically dilute, the effect of these artifacts can be considered to be linearly independent to the first order. Thus, these diagrams can be represented by any equivalent topology that does not violate the linearity principle (e.g., Fig. 2d,e). Although any number of alternate topologies may be correct mathematically, some may be more useful practically when developing procedures to correct EM measurements for common artifacts. For example, the topology in Fig. 2e shows more clearly how the effect of A_s and A_c can be corrected for simultaneously by subtracting the $EM[n]$ of a representative "blank" sample that contains both of these artifacts, such as filtered seawater (arrow labeled "1"). In these blanks, A_c would represent the contribution of background fluorescence and A_s would represent any EX that is scattered into the emission detector by the instrument itself. One further deconvolution of the instrument response $h_f[n]$ is needed to isolate the photosynthetic kinetics of interest $h_p[n]$ (arrow "3") from this partially corrected $EM[n]$ (arrow "2").

Determining the instrument (impulse) response of a Fasttracka FRRF—As shown by Fig. 2, the impulse response $h_f[n]$ is needed to compute the actual EM from any apparent EM measured by an instrument with a non-negligible dynamic artifact. Correction using $h_f[n]$ often is performed when a signal of

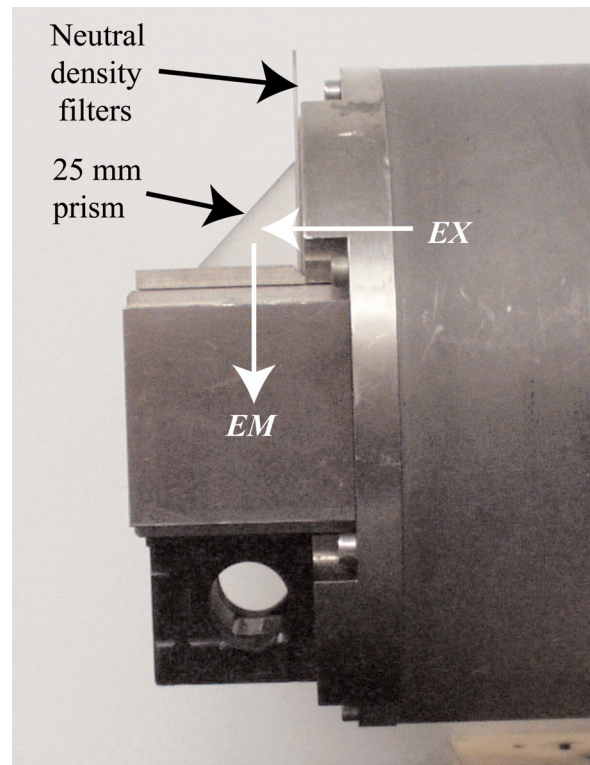


Fig. 3. The prism/filter configuration used to determine $h_f[n]$ of a Chelsea Marine Systems Fasttracka fluorometer. The prism redirects the excitation irradiance (EX) of the "light" chamber of the instrument into its detector, where it is measured as an apparent fluorescence emission (EM). This EX can be attenuated using different combinations of filters to determine $h_f[n]$ within and between instrument gain settings.

interest changes on time scales comparable to those of the instrument's response, such as in microstructure profiling of ocean temperature (e.g., Nash et al. 1999). Measuring EM with the Fasttracka FRRF is analogous in the sense that $h_f[n]$ and $h_p[n]$ both affect EM on similar time scales.

We developed a method to determine the $h_f[n]$ of a Fasttracka FRRF that requires only a 25 mm glass prism (Edmund Optics NT32-337) and different combinations of 2" square neutral density filters (Edmund Optics, kit p/n G54-460 or G55-222). By placing a prism in an instrument's sample area (Fig. 3), excitation flashlets can be redirected into its fluorescence detector aperture. A Fasttracka records this redirected excitation $EX[n]$ as an apparent fluorescence $EM[n]$ because the intensity of this redirected EX is much greater than what the emission filters on the detector were designed to block. Neutral density filters placed in the optical path attenuate the intensity of the redirected excitation and, therefore, the apparent EM that is measured. Different combinations of filters can be used to determine $h_f[n]$ across a range of different detector gain settings and at intervals within a given gain. This method does not require liquid standards, is repeatable over long periods of time, and, in theory, can be applied to any fluorometer whose excitation can be redirected into its fluorescence detec-

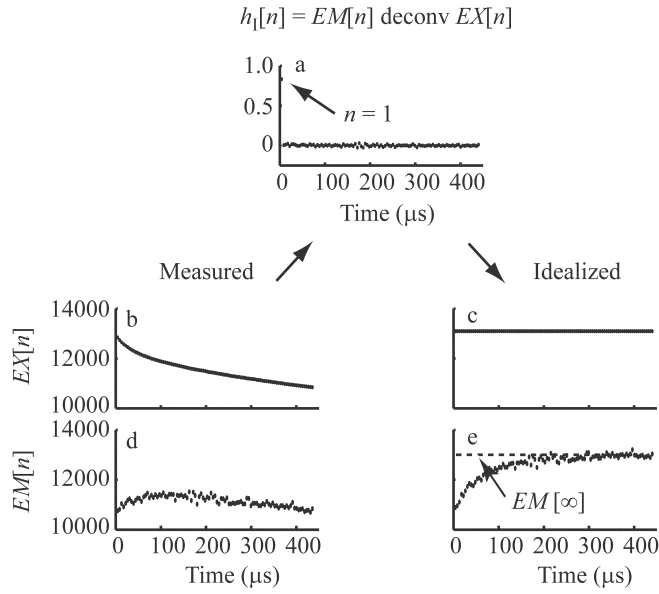


Fig. 4. Computing the idealized step response in EM from the dynamic instrument response $h_i[n]$. The $h_i[n]$ (a) is first determined by deconvolving a measured $EX[n]$ (b) from the $EM[n]$ (d) measured on a “sample” of a prism and neutral density filter(s). This $h_i[n]$ is then reconvolved with an idealized EX step function (c) to predict the instrument’s step response (e) at a given instrument gain setting. A multi-exponential equation like Eq. 1 then can be fit to the predicted EM transient to determine the time constants associated with this response. $EM[\infty]$ represents the asymptotic value that this predicted EM step response may or may not attain by the end of a given flash sequence. The EX and EM sequences used in this particular example are those shown in Fig. 1.

tor using a prism, optical fiber, or another approach.

This prism-filter combination is optically analogous to the two-element system in Fig. 2b, where the “fluorophore” in this case can be described by a scalar transfer function A_{p+F} . The instrument response $h_i[n]$ can be computed directly from the measured apparent $EM[n]$ by deconvolving $EX[n]$ from it to form $A_{p+F} \times h_i[n]$. We performed this deconvolution using the *deconv* routine in Matlab (The Mathworks). This routine requires as input a reflected, $2n-1$ length array of EM , which we created by concatenating $EM[n..1]$ to $EM[1..n]$ and removing the last element. The *deconv* routine determined $h_i[n]$ by deconvolving $EX[n]$ from this $2n-1$ array. This instrument response then was normalized to unity gain to correct for the gain introduced by A_{p+F} and for any gain or loss implicit in $h_i[n]$. Such normalization is appropriate because only the instrument’s dynamic response is of interest, not its gain or loss to EM .

Generating an idealized step response from the impulse response—The dynamic response of high speed optical detectors and the amplifying circuitry that follows them is described commonly in terms of their step response to a sudden shift from zero input to some level. These step responses often exhibit clear exponential behavior with multiple time scales (Kume 1994; Graeme 1996). To determine if the detector of this FRRF displayed simi-

lar behavior, we computed its step response to an idealized $EX[n]$ sequence of uniform flashlet intensity (Fig. 4c) by convolving this $EX[n]$ with the $h_i[n]$ (Fig. 4a) that we determined from sequences of $EX[n]$ and $EM[n]$ (Fig. 4b,d) that we measured with a prism with different neutral density filter combinations.

These idealized step responses then were fit with a general model for high-speed detectors

$$EM[n] = EM[\infty] \cdot \left(1 - \alpha_1 \cdot e^{-\frac{n}{\tau_1}} - \alpha_2 \cdot e^{-\frac{n}{\tau_2}} - \alpha_3 \cdot e^{-\frac{n}{\tau_3}} \dots \right) \quad (1)$$

that quantifies the dynamic instrument artifact in terms of different time scales τ with associated weights α that sum to unity. Equation 1 describes how the measured EM of a real instrument eventually rises asymptotically to the $EM[\infty]$ that an ideal instrument would attain instantaneously in the limit where all of the time constants τ approach zero (Fig. 4e). If the n in Eq. 1 is not a sample index per se but rather indicates a discrete point in units of time, then the τ in this equation will have units of time as well.

Assessment

The step response of a Fasttracka FRR fluorometer—We measured the instrument response of a particular FRR fluorometer (serial 014) in the laboratory at each of the four lowest detector gains ($\times 1$, $\times 4$, $\times 16$, and $\times 64$), using between five and nine different neutral density filter combinations with corresponding optical densities between 0.1 and 2.0. The most sensitive gain setting ($\times 256$) was not examined due to its low signal-to-noise ratio. The FRRF was oriented horizontally with its “light” chamber facing upward and with its sun block removed (see Fig. 3). The optical head was covered with a dark cloth to minimize any influence of ambient light. Since both of the sample chambers of this FRRF share a single detector, it is necessary only to measure the instrument response for one, in this case the light chamber, which can accommodate the prism and neutral density filters most easily.

The idealized step responses of this particular fluorometer exhibited multi-exponential kinetics on the single-turnover time scale at all four detector gains. These responses were well fit by a version of Eq. 1 having three time scales. The first time scale τ_1 was defined to be very short in this model, 0.001 of the time step between $EM[0]$ and $EM[1]$, to replicate the observed near-instantaneous initial rise in EM to $\approx 0.8 \times EM[\infty]$. The two longer-scale time constants τ_2 and τ_3 describe how the step response eventually rises toward $EM[\infty]$ over the remainder of the flashlet sequence, as in Fig. 4e.

Using a curve fitting procedure, the parameters of Eq. 1 were estimated for 27 different step responses across these four gain settings (Table 2). Differences in the dynamic instrument response within and between detector gains are difficult to resolve in $EM[n]$ by eye, but become apparent using this type of analysis. In general, both τ_2 and τ_3 contributed approximately equally to the gradual rise in EM to $EM[\infty]$. In many cases, the measured EM at the end of the flashlet sequence did not attain $EM[\infty]$. Because Eq. 1 is nonlinear, there is no sta-

Table 2. Estimates of the parameters of Eq. 1 as determined for different prism/filter combinations

Gain	Filter (OD)	τ_1	τ_2	τ_3^*	α_1	α_2	α_3	EM [∞]
1	0.1	0.001	25.48	104.53	0.84	0.07	0.10	15838
	0.2	0.001	32.95	133.28	0.84	0.09	0.07	11315
	0.3	0.001	26.95	122.45	0.83	0.08	0.09	10466
	0.4	0.001	33.29	122.59	0.85	0.08	0.08	7331
	0.5	0.001	37.94	133.23	0.84	0.09	0.07	5232
	0.6	0.001	31.28	107.63	0.84	0.07	0.10	3753
	1.0	0.001	43.59	102.53	0.84	0.08	0.08	1514
4	0.6	0.001	25.23	113.87	0.83	0.07	0.10	14357
	0.7	0.001	28.75	121.22	0.82	0.09	0.10	10185
	0.8	0.001	23.54	98.31	0.83	0.06	0.11	8483
	0.9	0.001	26.34	106.02	0.82	0.08	0.09	6123
	1.0	0.001	29.85	171.99	0.82	0.10	0.08	4414
	1.1	0.001	30.94	164.65	0.82	0.10	0.08	3618
	1.2	0.001	28.13	119.14	0.82	0.09	0.09	3296
	1.3	0.001	32.34	86.71	0.84	0.06	0.11	2857
	1.4	0.001	37.14	192.26	0.83	0.11	0.06	2047
	16	1.1	0.0011	27.28	159.28	0.81	0.09	0.10
1.2		0.0011	40.75	141.11	0.82	0.11	0.07	9950
1.3		0.001	25.37	208.17	0.78	0.13	0.09	7265
1.4		0.0011	24.83	181.64	0.81	0.11	0.08	6273
1.5		0.001	46.09	100.89	0.82	0.11	0.07	5924
1.6		0.001	45.11	182.38	0.75	0.16	0.09	3020
64	1.6	0.001	30.69	269.40	0.80	0.09	0.11	12393
	1.7	0.001	25.63	<i>300.00</i>	0.77	0.12	0.11	10597
	1.8	0.001	29.03	<i>300.00</i>	0.77	0.13	0.09	8113
	1.9	0.001	42.57	164.44	0.83	0.09	0.09	6419
	2.0	0.001	47.68	156.44	0.81	0.13	0.07	4967

*Fitted values presented in italics indicate estimates that equal a preset upper fitting limit and which are presumably incorrect.

tistically robust method for determining the confidence intervals of the estimates of these seven parameters (Press et al. 1992). A one-way analysis of variance (ANOVA) of each τ and α indicated that only the medium-scale time constant τ_2 and the long-scale weight α_3 differed significantly within and among these gain settings at the 0.05 level.

The estimates of $EM[\infty]$ that come from fitting this model to these computed step responses can be used to determine the actual gain of the instrument's fluorescence detector at each nominal gain setting. To do this, the optical densities D of Table 2 (a logarithmic scale) first must be converted into transmittances T (a linear scale) using the relationship $D = \log_{10}(T^{-1})$ (Kirk 1994). The relationships between T and $EM[\infty]$ at each of the four gain settings (Model II linear regressions, geometric mean method) (Laws and Archie 1981) were found to be scale with one another with the proportions 1.00, 2.71, 6.90, and 23.98 (Fig. 5). The most recent factory calibration of this instrument reported gain coefficients of 1.00, 3.09, 9.36, and 27.04, but, as the calibration method used by the manufac-

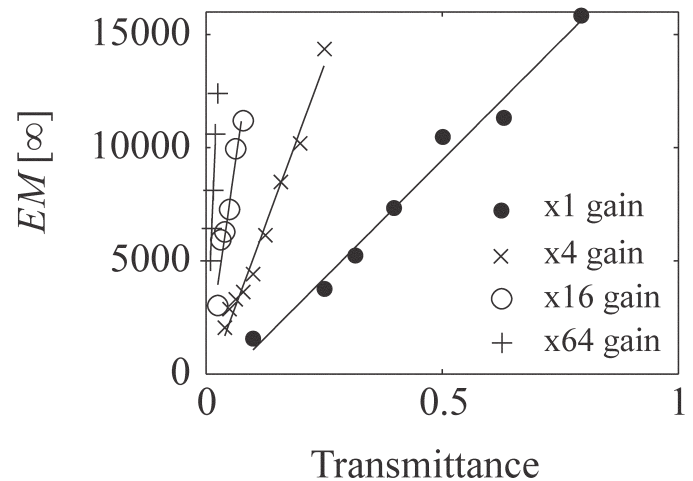


Fig. 5. Correlations between transmittance and $EM[\infty]$ at each of the four instrument gains, for a range of neutral density filters within different gain settings. Lines indicate Model II geometric mean regressions within each gain.

turer to compute these coefficients has not been published, we cannot objectively compare these two sets of coefficients.

A corrective method for Fasttracka EM in an oligotrophic region— Using this signal analysis framework and our technique for determining $h_i[n]$, we developed an artifact correction method for the Fasttracka which we assessed in November 2005 during a field study at Station ALOHA (22°45'N, 158°00'W) in the North Pacific. Near-surface phytoplankton assemblages were sampled continuously by directing the ship's uncontaminated supply (≈ 5 m depth) through the instrument's dark chamber, and measurements of $EM[n]$ and $EX[n]$ were taken every 13 s for approximately 6 d. Each measured $EM[n]$ or $EX[n]$ transient represented the average of 16 individual acquisitions computed internally by the instrument. A detector gain of $\times 64$ was used due to the very low levels of algal biomass. Chlorophyll a (Chl a) concentrations typically were between 7 to 8 ng L⁻¹ in these near-surface assemblages.

Concurrently with these measurements on unfiltered seawater, we also collected a time series of environmental blanks (Cullen and Davis 2003) using a system we designed that periodically redirected the continuous seawater supply through a 0.2 μ m filter (CritiCap-50, Pall Gelman Sciences). This system consisted of solenoid valves (Rainbird 100-DV) actuated by a custom-designed electronic driver that was, in turn, controlled by a timer program running on a computer to operate for 4 min every hour. The driver also output a voltage signal to indicate when the seawater supply was being filtered, which was recorded using the instrument's pressure sensor input to embed the timing of this filtering directly into the data record. During each hourly 4 min interval, approximately 19 of these "filtered" EX and EM sequences were measured, and each group of these 19 was averaged to compute a mean hourly $EX[n]$ and filtered $EM[n]$ transient. These filtered EM are anal-

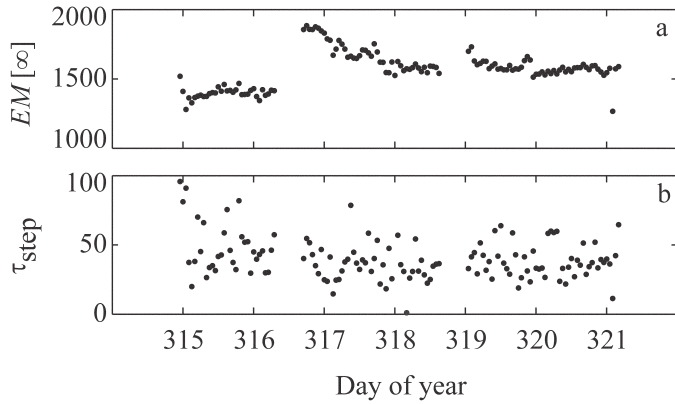


Fig. 6. Changes over 6 d in the apparent fluorescence of 0.2 μm filtered seawater at Station ALOHA, measured with a Fasttracka FRRF, in terms of (a) estimates of $EM[\infty]$ and (b) estimates of τ_{step} . The seawater supply was interrupted for short periods on days 316 and 318.

ogous to the signal arriving at the top of the summing junction in Fig. 2e (arrow “1”) and contain information about the background fluorescence in the filtered seawater (A_c), the instrument impulse response $h_i[n]$, and optical crosstalk due to EX scattering inside the dark chamber (A_s).

The instrument response $h_i[n]$ was determined from these hourly filtered averages by deconvolving $EX[n]$ from the apparent measured $EM[n]$ to form $(A_s + A_c) \times h_i[n]$, using the *deconv* routine as described above (see Fig. 2c). These then were scaled to unity gain to obtain the normalized impulse response. Then, the idealized step response of this instrument was generated for each hourly average “blank” by convolving each $h_i[n]$ with an idealized $EX[n]$ sequence of uniform flashlet intensity, as in Fig. 4. This resulted in an hourly time series that could be parameterized with a functional form similar to Eq. 1, so that we could monitor and quantify changes over time in the instrument response and in the magnitude of the background contribution to EM .

The signal-to-noise ratio of these EM blanks was low despite considerable averaging (effective $n_{\text{ave}} = 304$ for each hourly filtered blank). As a result, the three-exponential form of Eq. 1 that was used in the laboratory characterization did not provide robust fits to these hourly idealized step responses. For parameterizing these environmental blanks, a simpler two-exponential form was used instead:

$$EM[n] = EM[\infty] \cdot \left(1 - \alpha_1 \cdot e^{-\frac{n}{\tau_1}} - \alpha_{\text{step}} \cdot e^{-\frac{n}{\tau_{\text{step}}}} \right) \quad (2)$$

Here, τ_1 again represents the near-instantaneous rise to $EM[1]$, and the second time constant τ_{step} characterizes the increase in EM toward $EM[\infty]$ over the remainder of the flash sequence.

We observed considerable hours to days scale variability in the τ_{step} and α_{step} that were estimated by fitting Eq. 2 to our filtered, hourly $EM[n]$ time series (Fig. 6). This reflected changes in either the instrument response (τ_{step} , α_{step}) or in the magnitude of the filtered seawater background artifact ($EM[\infty]$). The magnitude of $EM[\infty]$ in these hourly filtered samples ranged

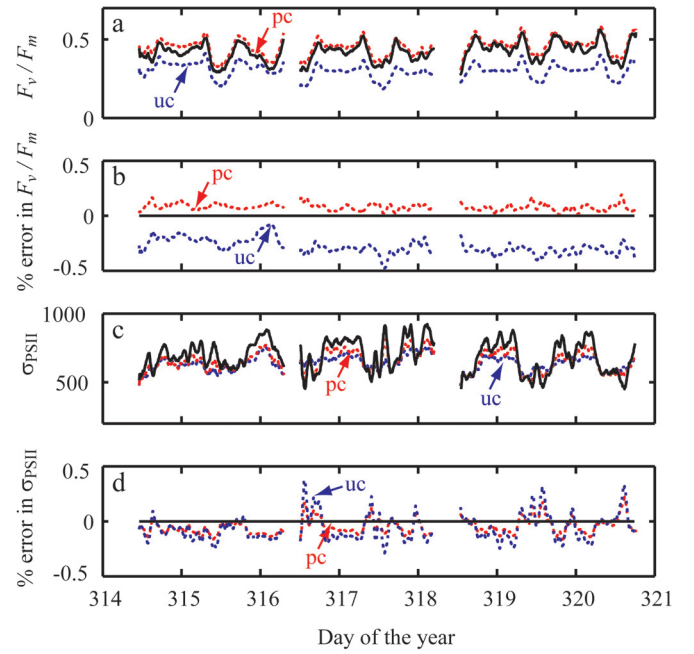


Fig. 7. Differences in time series of estimated F_v/F_m and σ_{pSII} over 6 d at Station ALOHA, as a function of the corrective method used. Solid lines in (a) and (c) represent parameter estimates from EM transients corrected both for background blanks and for instrument response artifacts. Dashed lines represent estimates from uncorrected EM data (“uc,” blue traces) and from EM data partially corrected only for the static blank background signal (“pc,” red traces). The percent errors incurred by applying no or only a partial correction are shown in (b) and (d) for F_v/F_m and σ_{pSII} , respectively.

between ≈ 1300 and 1900 (instrument units) over these 6 d (Fig. 6a), approximately 10% of the maximum emission signal that could be measured with the excitation protocol we used. However, because the average EM signal recorded during this field study in the unfiltered samples rarely exceeded 5,000, these background artifacts effectively represented about one-third of the measured EM . No clear trends were evident in the substantial fluctuations in $EM[\infty]$ over this period. These fluctuations presumably reflected changes in the EM contribution by dissolved background fluorescence because they were not correlated with changes in τ_{step} , which more closely reflects the instrument response (Fig. 6b). The average τ_{step} in these filtered field samples was $41 \pm 16 \mu\text{s}$, statistically indistinguishable from the average τ_2 of $35 \pm 1 \mu\text{s}$ of this fluorometer as determined by laboratory characterization (see Table 2).

We used these hourly $h_i[n]$ from the filtered measurements to correct the $EM[n]$ of unfiltered seawater for both instrument and sample artifacts. The sequence of operations for doing this was determined by following the signal path of Fig. 2e in reverse. First, the hourly filtered average $EM[n]$ (signal “1”) was subtracted element-wise from each unfiltered $EM[n]$ in the preceding and following 30 min. This provided an EM signal corrected for the environmental background fluorescence and scatter artifacts (signal “2”). Then, the nearest hourly impulse response was deconvolved from this signal as

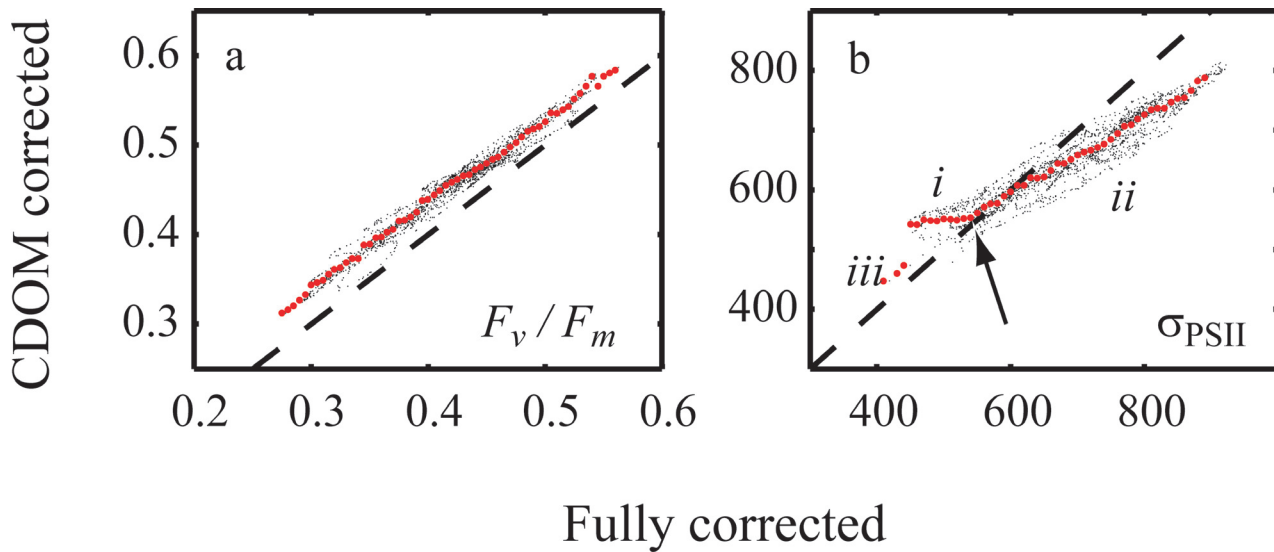


Fig. 8. Details of the errors shown in Fig. 7. (a) Estimates of F_v/F_m made without correcting for the dynamic artifact in $EM[t]$ (a, ordinate) are always higher than their fully corrected counterparts (a, abscissa), independent of the actual magnitude of the fully corrected F_v/F_m . Small dots represent all data points over the 6 d study, and larger red dots show the trend in the same data binned on 0.005 intervals. (b) A similar analysis of σ_{PSII} shows distinct trends that include overestimation (*i*) and underestimation (*ii*), with the σ_{PSII} data here being binned on intervals of ten.

before to compute an $EM[t]$ free from instrument artifact (signal “3”). Then, estimates of F_v/F_m and σ_{PSII} were computed from these corrected $EM[t]$ transients and their corresponding $EX[t]$ using software written by one of the authors (“v6,” S.R.L.), a more recent version of the $F(t)$ analysis software described in Laney (2003).

Static and dynamic artifacts in these field data affected estimates of F_v/F_m and σ_{PSII} differently. Not correcting for the static background artifacts in $EM[t]$ resulted in underestimates of F_v/F_m (Fig. 7a, “uc” for “uncorrected”) for the reasons explained by Cullen and Davis (2003). In addition, the dynamic instrument response keeps EM artifactually low during the beginning of flashlet sequence, which causes F_o to be underestimated more strongly than F_m . This results in a tendency to overestimate F_v/F_m when background contributions are corrected for but when the dynamic instrument artifact is not (Fig. 7a, “pc” for “partially corrected”). In these field data, the overestimates in F_v/F_m were as high as 22% (Fig. 7b). With σ_{PSII} , the main source of error is not the background contribution but rather the instrument response. Partially correcting for background fluorescence alone had only a minimal effect on estimates of σ_{PSII} (Fig. 7c, “pc”) and failed to correct the up to 16% underestimates and up to 22% overestimates in σ_{PSII} (Fig. 7c,d).

The error in partially corrected estimates of F_v/F_m generally was independent of its presumed correct value, i.e., the F_v/F_m that was estimated from the fully corrected $EM[t]$ transients. Partially corrected estimates of F_v/F_m were greater than fully corrected estimates by a constant amount (Fig. 8a). The error in partially corrected σ_{PSII} was more complex but still consistent with our analytical framework. A clear switch between overestimation and underestimation occurred at $\approx 550 \text{ \AA}^2 \text{ photon}^{-1}$

(Fig. 8b), which is the low end of the range of apparent σ_{PSII} that would be estimated by fitting the Kolber et al. (1998) variable fluorescence model to the hourly “filtered” measurements of $EM[t]$. In other words, this instrument, using this particular saturation flashlet protocol, would predict a σ_{PSII} of $\approx 550 \text{ \AA}^2 \text{ photon}^{-1}$ in the absence of any phytoplankton. When phytoplankton are present, the relationship between their actual σ_{PSII} and the instrument’s apparent σ_{PSII} determines whether or not the actual phytoplankton σ_{PSII} is overestimated or underestimated. Phytoplankton with a σ_{PSII} less than this $550 \text{ \AA}^2 \text{ photon}^{-1}$ threshold would exhibit EM transients that rise faster than the dynamic response of the instrument. The detector circuitry would effectively filter this faster response out, and the instrument would record its apparent σ_{PSII} of $550 \text{ \AA}^2 \text{ photon}^{-1}$ for all actual σ_{PSII} less than this threshold (region *i*).

For phytoplankton with actual σ_{PSII} above this threshold, the measured transients in EM would contain curvature that reflects photosynthetic physiology and the instrument response both (region *ii*). The instrument response adds curvature to EM earlier in the transient than where it would occur due to a photosynthetic physiology with a large σ_{PSII} , which would make EM appear to saturate sooner. A fitting algorithm would interpret these faster kinetics in EM as reflecting a smaller σ_{PSII} and therefore underestimate actual σ_{PSII} . There are too few data at the lowest end of the scale (region *iii*) to determine with confidence why those estimates of σ_{PSII} behave differently than those in region *i* or *ii*. It should be stressed that the particular threshold we observed here ($550 \text{ \AA}^2 \text{ photon}^{-1}$) is a function of the specific excitation protocol used in this study and of the instrument’s EX calibration. Thus, this threshold has meaning only in a relative sense for a single instrument at

a given protocol, and cannot be used to compare necessarily among different instruments or protocols in an absolute sense.

Discussion

Oceanographic relevance—Correction for measurement artifacts is a necessary but often neglected part of using variable fluorescence techniques properly. Cullen and Davis (2003) demonstrated how uncorrected background artifacts in DCMU-based measurements of F_o and F_m can bias, inadvertently, ecological interpretations of observed variability in F_v/F_m and how these static artifacts can be corrected for by measuring and subtracting appropriate “blanks.” When F_o , F_m and other physiological parameters are estimated from the kinetics of variable fluorescence transients, however, dynamic artifacts also must be considered and corrected for if necessary. Dynamic artifacts distort the time course with which F increases from F_o to F_m during the transient measurement, and this distortion tends to affect estimates of F_o and F_m unequally. Such distortion cannot be corrected for algebraically using a simple blanking approach, and more sophisticated mathematical manipulations are required.

Tools and techniques from signal analysis can help identify exactly how a given static or dynamic artifact affects measured $EM(t)$ or $EX(t)$, and what measurements must be collected to correct for their effect. Diagrams such as those in Fig. 2 can be used to determine which among several possible corrective approaches is the most feasible or practical in any given measurement situation, simplifying the overall corrective process. We have classified artifacts according to their physical source (“sample” versus “instrument”) and their effect on EM (“static” or “dynamic”), more rigorously than is used often in the treatment of “blanks.” Such detail can provide insight into the relative contribution of specific artifacts and better show how each artifact affects the ultimate physiological parameters of interest, information which often is lost when considering artifacts from the perspective of simple blanks.

Appropriate correction of measured EM transients ultimately depends on knowing the transfer function of every artifact that is significant in a given situation. However, many potentially important artifacts might affect EM in ways that are difficult to determine empirically. For example, it is challenging to separate the actual fluorescence of particles in a sample from an apparent fluorescence that actually is scattering of EX . In situations where these less tractable artifacts must be considered, modeling or estimation (e.g., Laney et al. 2001) can be used to approximate their probable effect on EM . Then, this information can be used to develop a transfer function for use with an appropriate corrective procedure.

This study examined only a few of the many artifacts that can potentially affect $F(t)$ measurements in laboratory cultures or in natural samples. We focused largely on a dynamic artifact in a particular fluorometer, but it is important to note that dynamic artifacts also can arise from non-instrument sources. For example, the ambient light field near the ocean

surface contains considerable irradiance in the chlorophyll fluorescence wavelengths that will not be blocked by emission filters on the fluorescence detector. For sample volumes exposed to the ambient light field (such as those in the “light” chamber of this Fasttracka fluorometer), this irradiance will modulate the measured EM on the μ s to ms time scale. Measurement artifact due to such solar contamination currently limits our ability to examine photosynthetic behavior in the top optical depths under ambient light conditions. However, variable fluorescence measurements in these depths are critical to understanding better the environmental variability of related properties like sun-stimulated fluorescence (Laney et al. 2005). An appropriate signal diagram will show how this dynamic artifact can be corrected for if the ambient irradiance can be measured simultaneously with the same temporal resolution as EM and EX . Any future approach for measuring variable fluorescence in the natural light field can use the signal analysis framework we present here to develop a corrective approach for this important, yet currently unaddressed, dynamic artifact in EM .

By improving the Fasttracka’s detector circuitry, it may be possible to reduce or even make negligible the specific dynamic artifact that we examined in this study. Nevertheless, a considerable amount of $F(t)$ data has been already collected with these instruments and accurately interpreting these data will require a robust corrective approach like the one presented here. Advances in optoelectronics have made it easier to develop instruments and prototypes for measuring variable fluorescence transients (e.g., Koblížek et al. 2001; Fuchs et al. 2002; Johnson 2004), and dynamic instrument artifacts may or may not be negligible in instruments that incorporate such newer technology. It is difficult to assess the effect of instrument artifacts in new instruments because their description rarely includes characterization data that either quantify such artifacts or demonstrate that they are negligible. When describing new instruments or prototypes, authors are encouraged to present results of simple characterization studies that examine the potential effect of such dynamic artifacts.

Practical issues—Users who require a high degree of precision or accuracy in variable fluorescence transients might consider applying some of the approaches we have described here. Our prism and filter technique improves on one suggested by Laney (2003) for determining the impulse response of a Fasttracka. This previous technique required a series of liquid dye standards that may be more difficult to handle and that may be less stable than the more optically inert prisms or filters over time. With our approach, one can measure the dynamic response of a fluorescence detector at precise and repeatable increments, making it possible to determine the actual gain of an instrument at any nominal gain setting. The measurement geometry of other fluorometers may preclude using filters and prisms in the same fashion as we have here, but our general approach of redirecting attenuated excitation irradiance into the detector may be applicable nonetheless.

The automatic valve system we developed for our field assessment represents one possible approach to monitoring instrument and sample artifacts in continuous flow systems. At Station ALOHA, approximately one-third of the EM measured in surface samples represents a background artifact, and thus relatively minor changes in the background signal introduce comparatively large errors in the photosynthetic properties that are estimated from $F(t)$. The up to 50% day-to-day changes in the background artifact over this 6-d study underscore the importance of monitoring any background contribution and correcting for it if necessary. We did not conduct a similar study in a meso- or eutrophic region, but we expect that the relative contribution of artifacts in such regions will differ from those at Station ALOHA, perhaps strongly. A further study of artifacts in $F(t)$ in these other water types would be a valuable complement to the findings presented here.

Our valve system allowed us to measure environmental “blanks” automatically in a continuous flow system. It also is possible to process discrete samples similarly by separately preparing and measuring filtered and unfiltered pairs of samples. This is probably the most robust procedure for obtaining precise correction for artifacts when using this particular instrument, given that its dynamic artifact displayed no clear trend that could be parameterized readily (Table 2 and Fig. 6). This approach would be cumbersome, but may be necessary in certain situations, such as when the dissolved background signal is expected to form a considerable portion of the apparent measured EM (Fuchs et al. 2002; Cullen and Davis 2003). In general, it is advisable to assess the probable sources of error in any given measurement and first determine which one is dominant before applying such a labor-intensive corrective approach. In many situations, the benefits gained by applying such an involved corrective approach may not improve the overall error in the final estimates of F_o , F_m , σ_{PSII} , τ , and ρ materially, especially if the dominant source of artifact is not accurately represented in the correction.

Comments and recommendations

When using variable fluorescence techniques based on the measurement of transients, dynamic sources of artifact must be considered in addition to static artifacts such as background fluorescence or instrument offset. Given the large errors that dynamic artifacts can introduce in derived photosynthetic parameters, readers should view reports with caution that fail to discuss how these artifacts were quantified and either shown to be negligible or corrected for. We reiterate Cullen and Davis's (2003) recommendation that analysts carefully examine and report sample blanks from their variable fluorescence studies. Our contribution is to stress that what is appropriate for a “blank” generally depends on the method and instrument used to measure variable F .

Our study focused on the Fasttrack instrument because it is arguably the most widely used single-turnover fluorometer in oceanographic studies at present. In many mea-

surement situations, its dynamic instrument artifact cannot be neglected, as is shown in our field assessment in the oligotrophic subtropical Pacific. The signal analysis framework that we apply here to variable fluorescence is not limited to this particular instrument, but rather is generally applicable to many other fluorescence techniques, not only those that stimulate a transient response, but also those that continuously force a fluorescence emission. As techniques for probing and interpreting the dynamic responses of chlorophyll variable fluorescence become more sophisticated, rigorous mathematical treatments of observed responses will become increasingly important to interpreting these responses accurately.

References

- Cullen, J. J., and R. F. Davis. 2003. The blank can make a big difference in oceanographic measurements. *Limnol. Oceanogr. Bull.* 12:29–35.
- Doebelin, E. O. 1990. *Measurement systems: application and design*, 4th ed. McGraw-Hill.
- Falkowski, P. G., K. D. Wyman, A. C. Ley, and D. C. Mauzerall. 1986. Relationship of steady state photosynthesis to fluorescence in eukaryotic algae. *Biochim. Biophys. Acta* 849: 183–192.
- Fuchs, E., R. C. Zimmerman, and J. S. Jaffe. 2002. The effect of elevated levels of phaeophytin in natural waters on variable fluorescence measured from phytoplankton. *J. Plankton Res.* 24:1221–1229.
- Genty, B., J.-M. Briantais, and N. R. Baker. 1989. The relationship between the quantum yield of photosynthetic electron transport and photochemical quenching of chlorophyll fluorescence. *Biochim. Biophys. Acta* 990:87–92.
- Graeme, J. G. 1996. *Photodiode amplifiers: op amp solutions*. McGraw-Hill.
- Johnson, Z. 2004. Development and application of the background irradiance gradient - single turnover fluorometer (BIG-STf). *Mar. Ecol. Prog. Ser.* 283:73–80.
- Kirk, J. T. O. 1994. *Light and photosynthesis in aquatic ecosystems*, 2nd ed. Cambridge University Press.
- Koblížek, M., D. Kaftan, and L. Nedbal. 2001. On the relationship between the non-photochemical quenching of the chlorophyll fluorescence and the Photosystem II light harvesting efficiency. A repetitive flash fluorescence induction study. *Photosyn. Res.* 68:141–152.
- Kolber, Z. S., O. Prasil, and P. G. Falkowski. 1998. Measurements of variable chlorophyll fluorescence using fast repetition rate techniques: defining methodology and experimental protocols. *Biochim. Biophys. Acta* 1367: 88–106.
- Kume, H. [ed.]. 1994. *Photomultiplier tube: principle to application*. Hamamatsu.
- Laney, S. R. 2003. Assessing the error in photosynthetic properties determined by fast repetition rate fluorometry. *Limnol. Oceanogr.* 48:2234–2242.

- , R. M. Letelier, and M. R. Abbott. 2005. Parameterizing the natural fluorescence kinetics of *Thalassiosira weissflogii*. *Limnol. Oceanogr.* 50:1499–1510.
- , R. M. Letelier, R. A. Desiderio, M. R. Abbott, D. A. Kiefer, and C. R. Booth. 2001. Measuring the natural fluorescence of phytoplankton cultures. *J. Atmos. Ocean. Tech.* 18:1924–1934.
- Laws, E. A., and J. W. Archie. 1981. Appropriate use of regression analysis in marine biology. *Mar. Biol.* 65: 13–16.
- Ley, A. C., and D. C. Mauzerall. 1986. The extent of energy transfer among Photosystem II reaction centers in *Chlorella*. *Biochim. Biophys. Acta* 850:234–248.
- Mauzerall, D. 1972. Light-induced changes in *Chlorella*, and the primary photoreaction for the production of oxygen. *PNAS* 69:1358–1362.
- Mitra, S. K. 2001. *Digital signal processing – A computer-based approach*, 2nd ed. McGraw-Hill.
- Nash, J., D. Caldwell, M. Zelman, and J. Moum. 1999. A thermocouple probe for high-speed temperature measurement in the ocean. *J. Atmos. Ocean. Tech.* 16: 1474–1482.
- Olson, R. J., A. M. Chekalyuk, and H. M. Sosik. 1996. Phytoplankton photosynthetic characteristics from fluorescence induction assays of individual cells. *Limnol. Oceanogr.* 41: 1253–1263
- Press, W. H., S. A. Teukolsky, W. T. Vetterling, and B. P. Flannery. 1992. *Numerical Recipes in C*. Cambridge University Press.
- Schiermeier, Q. 2007. Artefacts in ocean data hide rising temperatures. *Nature* 447:8–9.
- Willis, J. K., J. M. Lyman, G. C. Johnson, and J. Gilson. 2007. Correction to “Recent Cooling of the Upper Ocean.” *Geophys. Res. Lett.* 34, [doi:10.1029/2007GL030323].

Submitted 17 November 2006

Revised 11 September 2007

Accepted 21 September 2007